Itinerant and local-moment magnetism in $EuCr_2As_2$ single crystals

U. B. Paramanik,[1] R. Prasad,[1] C. Geibel,[2] and Z. Hossain[1,2,*]
[1]*Department of Physics, Indian Institute of Technology, Kanpur 208016, India*
[2]*Max Planck Institute for Chemical Physics of Solids, 01187 Dresden, Germany*
(Received 20 February 2014; revised manuscript received 14 April 2014; published 25 April 2014)

We report on the crystal structure, physical properties, and electronic structure calculations for the ternary pnictide compound $EuCr_2As_2$. X-ray diffraction studies confirmed that $EuCr_2As_2$ crystalizes in the $ThCr_2Si_2$-type tetragonal structure (space group $I4/mmm$). The Eu ions are in a stable divalent state in this compound. Eu moments in $EuCr_2As_2$ order magnetically below $T_m = 21$ K. A sharp increase in the magnetic susceptibility below T_m and the positive value of the paramagnetic Curie temperature obtained from the Curie-Weiss fit suggest dominant ferromagnetic interactions. The heat capacity exhibits a sharp λ-shape anomaly at T_m, confirming the bulk nature of the magnetic transition. The extracted magnetic entropy at the magnetic transition temperature is consistent with the theoretical value $R\ln(2S+1)$ for $S = 7/2$ of the Eu^{2+} ion. The temperature dependence of the electrical resistivity $\rho(T)$ shows metallic behavior along with an anomaly at 21 K. In addition, we observe a reasonably large negative magnetoresistance ($\sim -24\%$) at lower temperature. Electronic structure calculations for $EuCr_2As_2$ reveal a moderately high density of states of Cr-3*d* orbitals at the Fermi energy, indicating that the nonmagnetic state of Cr is unstable against magnetic order. Our density functional calculations for $EuCr_2As_2$ predict a G-type AFM order in the Cr sublattice. The electronic structure calculations suggest a weak interlayer coupling of the Eu moments.

DOI: 10.1103/PhysRevB.89.144423 PACS number(s): 74.70.Xa, 75.50.Cc, 75.40.Cx, 71.20.−b

I. INTRODUCTION

The layered pnictide intermetallic compounds RT_2Pn_2 (R = rare-earth elements, T = transition metal, Pn = pnictide) with $ThCr_2Si_2$-type tetragonal structure (space group $I4/mmm$) exhibit a rich variety of transport and magnetic properties. These compounds consist of alternate *T-Pn* layers and *R* layers stacked along the *c* axis. Following the exploration of these materials over the last 20 years, recently, the discovery of high-temperature superconductivity (SC) in the doped AFe_2As_2 (A = divalent alkaline metal or rare-earth metal) has generated a new wave of investigations in search of new compounds in this class, which exhibit interesting magnetic and superconducting properties. The Fe atoms in these materials undergo a spin-density-wave (SDW) antiferromagnetic (AFM) transition below 200 K. Upon doping or under application of external pressure, the Fe AFM ordering weakens and SC emerges [1–5].

Europium is among the few special rare-earth elements having two stable valence configurations: Eu^{2+} ($J = S = 7/2$) and Eu^{3+} ($J = 0$); Eu^{2+} bears a strong magnetic moment ($\sim 7.0\ \mu_B$) whereas Eu^{3+} does not carry any moment. In a few cases a mixed-valence state of Eu is also observed, for example, in $EuNi_2P_2$ and $EuCu_2Si_2$ [6–8]. $EuFe_2As_2$ is a member of the Fe-based 122 pnictide family where Eu is divalent. This system undergoes a SDW transition in the Fe sublattice at 190 K accompanied by an AFM ordering of Eu^{2+} moments at 19 K [9]. The interplay between SC and Eu^{2+} magnetism in doped $EuFe_2As_2$ has been extensively studied recently [4,5,9–12]. Replacing As by P in $EuFe_2P_2$, no Fe moment has been observed in the system and the divalent Eu moments order ferromagnetically at $T_c = 30$ K as has been detected by neutron diffraction measurements [13,14]. Incommensurate antiferromagnetic structure of Eu^{2+} moments with $T_N = 47$ K has been found in $EuRh_2As_2$ [15]. While $EuCu_2As_2$ exhibits a delicate balance between FM and AFM ordering [16], $EuNi_2As_2$ and $EuCo_2As_2$ order antiferromagnetically [17,18]. Briefly, the pnictide compounds of this structure class show a variety of novel and interesting behaviors.

We synthesized the isostructural compound $EuCr_2As_2$. This compound crystalizes in the $ThCr_2Si_2$-type tetragonal structure with space group $I4/mmm$. As shown in Fig. 1, alternating Eu layers and CrAs layers are stacked along the *c* axis where Cr atoms form a square planar lattice in the CrAs layer, similarly to AFe_2As_2. Recently, Singh *et al.* have investigated the closely related compound $BaCr_2As_2$ [19]. A combined study of physical properties and electronic structure calculations demonstrates that $BaCr_2As_2$ is a metal with itinerant antiferromagnetism, similar to the parent phases of Fe-based superconductors but with slightly different magnetic structure. Neutron diffraction measurements on $BaFe_{2-x}Cr_xAs_2$ crystals reveal that the Cr doping in $BaFe_2As_2$ leads to suppression of the Fe SDW transition but the superconductivity (as usually observed in the case of other transition metal doping) is prevented by a new competing magnetic order of G-type antiferromagnetism which becomes the dominant magnetic ground state for $x > 0.3$ [20,21]. $BaCr_2As_2$ shows stronger transition metal–pnictogen covalency than the Fe compounds [19] and in that respect is more similar to the widely studied compound $BaMn_2As_2$. $BaMn_2As_2$ has been characterized as a small-band-gap semiconductor with G-type AFM ordering of Mn moments at $T_N = 625$ K [22,23]. This material becomes metallic by partial substitution of Ba by K or by applied pressure on the parent compound [24–26]. In contrast to $BaCr_2As_2$ and $BaMn_2As_2$, both having tetragonal crystal structure, $EuMn_2As_2$ forms in a hexagonal crystal structure [27] whereas $EuCr_2As_2$ is found to be tetragonal. Very recently, the closely related compounds *Ln*OCrAs (*Ln* = La, Ce, Pr, and Nd) possessing similar CrAs layers

*zakir@iitk.ac.in

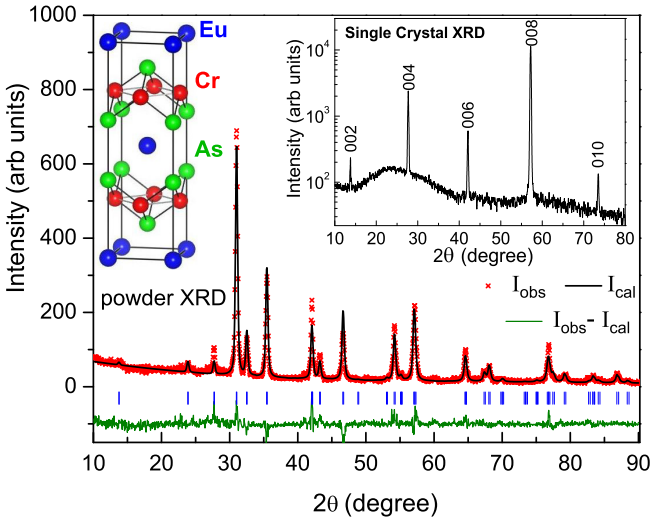

FIG. 1. (Color online) The powder x-ray diffraction pattern of $EuCr_2As_2$ recorded at room temperature. The Rietveld refinement fit (solid black line), difference profile (lower solid green line), and positions of Bragg peaks (vertical blue bars) are also shown. Inset: X-ray diffraction pattern for $EuCr_2As_2$ platelike single crystal.

as in $BaCr_2As_2$ have been synthesized by Park *et al.* [28]. These compounds are isostructural (ZrCuSiAs-type structure with the space group $P4/nmm$) to that of *Ln*OFeAs, which are the parent compounds of Fe-based high-T_c superconductors. Powder neutron diffraction measurements at room temperature reveal that Cr^{2+} ions in LaOCrAs bear a large itinerant moment of 1.57 μ_B pointing along the c axis which undergoes a G-type AFM ordering. The Néel temperature T_N has been estimated to be in between 300–550 K. Therefore, the related materials possessing CrAs layers are highly enthralling with regard to the physical properties when the AFM ordering is suppressed by doping.

Here we report on the crystal structure, physical properties, and electronic structure calculations of $EuCr_2As_2$. Our combined experimental investigations and density functional studies show that Eu ions are in a divalent state and the Eu^{2+} local moments order magnetically at $T_m = 21$ K. $M(T)$ and $M(H)$ data suggest competing FM and AFM interactions since the $M(T)$ curves look like that of a ferromagnet while the $M(H)$ curves lack the features typically observed in a ferromagnet. A large negative magnetoresistance is found below T_m. Density functional theory based calculations indicate that the Cr ions bear itinerant moments and the most stable magnetic state in the Cr sublattice is a G-type AFM order.

II. METHODS

The single crystals of $EuCr_2As_2$ were grown using CrAs flux as described by Singh *et al.* [19]. The CrAs binary was presynthesized by reacting the mixture of Cr powder and As pieces at 300 °C for 10 h, and then at 600 °C for 30 h and finally at 900 °C for 24 h. A ratio of Eu:CrAs = 1:4 was placed in an alumina crucible, and sealed inside a tantalum tube. The assembly was put into a furnace and heated to 1230 °C slowly and held there for 13 h, and then was cooled to 1120 °C at a rate of 2 °C/h; finally it was furnace-cooled to room temperature. The shiny platelike $EuCr_2As_2$ crystals were formed in layers, which were cleaved mechanically from the flux. Several platelike single crystals with typical dimensions $4 \times 4 \times 0.2$ mm^3 were obtained. The polycrystalline samples of $EuCr_2As_2$ were prepared using a solid state reaction method similar to that of $EuFe_2As_2$ as described in our earlier reports [4,9,11]. Stoichiometric amounts of the starting elements of Eu chips (99.9%), Cr powder (99.999%), and As chips (99.999%) were used for the reaction. The single crystals and crushed polycrystalline samples were characterized by x-ray diffraction (XRD) with Cu-K_α radiation to determine the single-phase nature and crystal structure. A scanning electron microscope (SEM) equipped with energy-dispersive x-ray (EDX) analysis was used to check the homogeneity and composition of the samples. The electrical transport properties were measured by the standard four-probe technique using a close cycle refrigerator (Oxford Instruments) and physical property measurement system (PPMS; Quantum Design). The $\chi(T) = M(T)/H$ and $M(H)$ isotherms were measured using a commercial SQUID magnetometer (MPMS; Quantum Design). The specific heat was measured by the relaxation method in a PPMS (Quantum Design).

We have carried out the density functional band structure calculations using the full potential linear augmented plane wave plus local orbitals (FP-LAPW + lo) method as implemented in the WIEN2k code [29]. The Perdew-Burke-Ernzerhof (PBE) form of the generalized gradient approximation (GGA) was used to calculate the exchange correlation potential [30]. Additionally, to correct the on-site strong Coulomb interaction within the Eu-4f orbitals we have included U on a mean-field level using the GGA + U approximation. No spectroscopy data for $EuCr_2As_2$ are available in the literature; therefore, we have used $U = 8$ eV, the standard value for an Eu^{2+} ion [4,9,31]. In addition, the spin-orbit coupling is included with the second variational method in the Eu-4f shell. The set of plane-wave expansion K_{MAX} was determined as $R_{MT} \times K_{MAX}$ equals 7.0 and the K mesh used was $10 \times 10 \times 10$.

III. RESULTS AND DISCUSSION

A. Crystal structure

Figure 1 shows the powder XRD pattern at room temperature for the crushed polycrystalline sample of $EuCr_2As_2$. All the diffraction peaks could be indexed based on the $ThCr_2Si_2$-type structure (space group $I4/mmm$). The crystallographic lattice parameters are listed in Table I. The c/a ratio for $EuCr_2As_2$ is much larger than that of other Eu-based transition-metal pnictides. A comparison of the structural parameters is shown in Table II. An increased c/a ratio has also been observed in the homologous compound $BaCr_2As_2$ ($a = 3.96$ Å and $c = 13.632$ Å) [19] as compared to other transition-metal compounds BaT_2As_2. The inset of Fig. 1 shows the x-ray diffraction pattern for a $EuCr_2As_2$ single crystal. Only the (00l) diffraction peaks are observed, confirming that the crystallographic c axis is perpendicular to the plane of the platelike single crystals. From the EDX analysis, the single-phase nature of the sample is manifested with an obtained atomic ratio of Eu:Cr:As as 20.8:38.3:40.9.

TABLE I. Crystallographic parameters obtained from the structural Rietveld refinement of powder XRD data of $EuCr_2As_2$. The refinement quality parameter $\chi^2 = 1.62$.

Structure		$ThCr_2Si_2$-type tetragonal		
Space group		$I4/mmm$		
Lattice parameters				
a (Å)		3.893(2)		
c (Å)		12.872(2)		
V_{cell} (Å^3)		195.08(1)		
Refined atomic coordinates				
Atom	Wyckoff	x	y	z
Eu	2a	0	0	0
Cr	4d	0	0.5	0.25
As	4e	0	0	0.363

B. Magnetic susceptibility and isothermal magnetization

Figure 2 shows the temperature dependence of the magnetic susceptibility $\chi_{ab}(T)$ for $EuCr_2As_2$ with the applied magnetic field $H = 1$ kOe along the crystallographic ab plane ($H \parallel ab$). There is a sharp increase in $\chi_{ab}(T)$ below 21 K which tends to saturate at lower temperature as in the case of a ferromagnetic order. At high temperature $\chi_{ab}(T)$ follows the modified Curie-Weiss behavior, $\chi(T) = \chi_0 + C/(T - \theta_P)$, where χ_0 is the temperature-independent term of the susceptibility, C is the Curie constant, and θ_P is the Weiss temperature. The fitting of inverse susceptibility data by the Curie-Weiss behavior in the temperature range 50–300 K (shown by the solid line) yields the effective paramagnetic moment $\mu_{\text{eff}} = 7.95\ \mu_B$ and $\theta_P = 19$ K. A similar fit for $\chi_c(T)$ data (not shown here) yields the effective paramagnetic moment $\mu_{\text{eff}} = 8.27\ \mu_B$ and $\theta_P = 22$ K. For both χ_{ab} and χ_c, the effective paramagnetic moments are close to the theoretical value of $g\sqrt{S(S+1)}\mu_B = 7.94\ \mu_B$ for free Eu^{2+} moments ($S = 7/2$, $L = 0$). The positive values of the paramagnetic Curie temperature θ_P obtained from the fit suggest predominantly ferromagnetic exchange interactions between the Eu^{2+} moments.

Figure 3(a) represents the magnetization $M(T)$ in two different orientations of magnetic field, i.e., $H \parallel ab$ and $H \parallel c$. At high temperature $M(T)$ is almost isotropic, as normally observed for a stable divalent Eu state. Since it bears a spin-only ($J = S = 7/2$) moment, one expects a negligible anisotropy. However, a significant anisotropy in the magnetization is developed below 25 K ($M_{H\parallel c}/M_{H\parallel ab} \approx 1.5$ at 21 K), suggesting an anisotropic magnetic interaction. The rapid increase of $M(T)$ below 21 K gives an impression that the magnetic order is either ferromagnetic in nature or has a strong ferromagnetic component. To gain further insight on the nature of the magnetic order we have carried out isothermal magnetization measurements with varying magnetic fields at fixed temperatures [Fig. 3(b)]. At temperature $T = 2$ K, the magnetization for $H \parallel c$ saturates more rapidly as the magnetic field is increased from $H = 0$ to 4.1 kOe. For $H \parallel ab$, the magnetization saturates at much higher field (18 kOe). A sizable magnetic field is required to achieve the saturation of magnetization for both $H \parallel ab$ and $H \parallel c$. We do not observe any hysteresis in the $M(H)$ curve at 2 K. It is known that a good quality single crystal of a ferromagnet

TABLE II. A comparison of the structural and magnetic parameters of $EuCr_2As_2$ with some isostructural Eu compounds. The lattice parameters a and c are at room temperature, T_N/T_C are the antiferromagnetic/ferromagnetic ordering temperatures, and μ_{eff} is the effective moment calculated from the Curie-Weiss fit of magnetic susceptibility data.

Compound	a (Å)	c (Å)	T_N/T_C (K)	μ_{eff} (μ_B/f.u.)	Ref.
$EuFe_2As_2$	3.907	12.114	19	7.79	[9]
$EuCu_2As_2$	4.260	10.203	15	7.90	[16]
$EuNi_2As_2$	4.096	10.029	14	7.30	[17,42]
$EuCo_2As_2$	3.934	11.511	39	7.40	[18,42]
$EuCr_2As_2$	3.893	12.872	21	7.95	This work

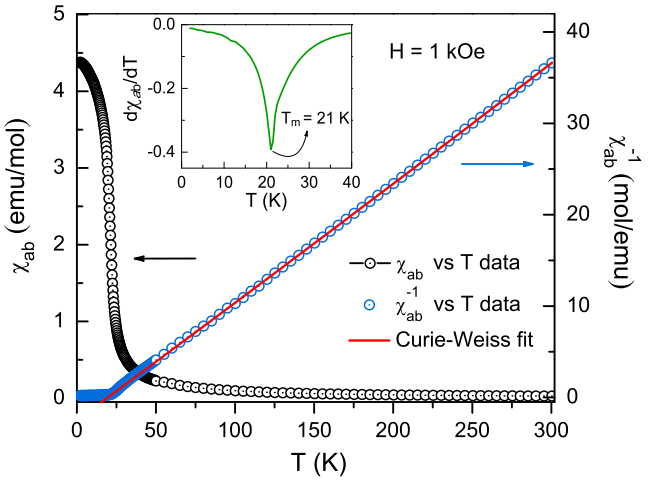

FIG. 2. (Color online) Temperature dependence of magnetic susceptibility χ_{ab} for $EuCr_2As_2$ with the applied magnetic field $H = 1$ kOe. The solid line represents the fit to the Curie-Weiss behavior.

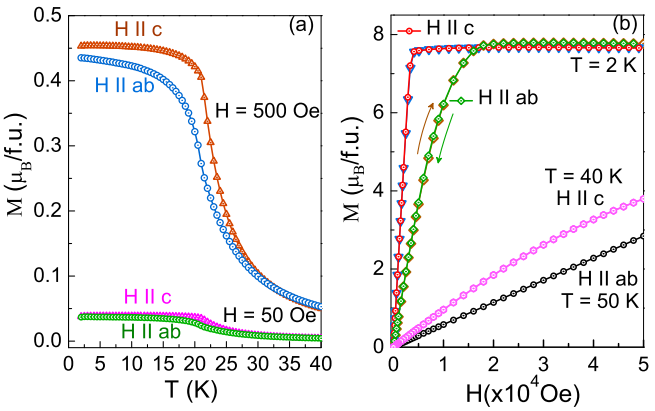

FIG. 3. (Color online) (a) Temperature dependence of magnetization M of $EuCr_2As_2$ single crystal under applied field of 50 Oe and 500 Oe with H in the ab plane ($H \parallel ab$) and parallel to the crystallographic c axis ($H \parallel c$). All the data shown are in zero-field-cooled (ZFC) condition. (b) Isothermal magnetization M of $EuCr_2As_2$ single crystal with $H \parallel ab$ and $H \parallel c$. M-H data were corrected for the demagnetization effect, taken on a platelike sample.

with small anisotropy and thus small domain wall energy may not always exhibit remanent magnetization [32]. Thus, one cannot rule out the possibility of a FM state of Eu^{2+} moments in $EuCr_2As_2$. However, combining the experimental results with the electronic structure calculations (to be discussed below), where we get an antiferromagnetic ground state of the interlayer Eu moments with very weak interlayer coupling, it is possible that the dominant nearest-neighbor (i.e., intralayer) Eu-Eu interaction is FM as indicated by a positive value of θ_P, but there could be a weak or frustrated AFM coupling between the layers. In this connection, we may recall other homologous compounds $EuCu_2As_2$ or $EuFe_2As_2$, wherein the intralayer Eu-Eu interaction has been established to be ferromagnetic, while the interlayer antiferromagnetic coupling is very weak [16,33–35]. If we consider the interlayer Eu-Eu antiferromagnetic coupling to be very weak in $EuCr_2As_2$, then, a small external magnetic field as employed in our magnetic measurements can reorient the spin arrangement along the field direction at the onset of magnetic ordering. The saturated magnetization at 2 K is determined to be $\sim$7.78 μ_B/f.u. and $\sim$7.66 μ_B/f.u. for $H \parallel ab$ and $H \parallel c$, respectively, implying that the system is nearly isotropic. The measured saturated magnetization for both the directions are more than that expected for parallelly aligned Eu^{2+} moments ($gS = 7.0$ μ_B/f.u. with $g = 2$, $S = 7/2$), indicating that the Cr ions carry an itinerant moment and are contributing to the total magnetization. The electronic structure calculations on $EuCr_2As_2$ (to be discussed below) also suggest that Cr carries an itinerant moment and the most stable magnetic structure in the Cr sublattice is a G-type AFM order. The homologous compound $BaCr_2As_2$ has been proposed to be a metal with itinerant antiferromagnetism [19]. In fact, neutron diffraction measurements on $BaFe_{2-x}Cr_xAs_2$ crystals reveal that for $x > 0.3$, the magnetic ground state is consistent with G-type AFM order [21]. It also suggests that the Cr magnetic ordering could be well above room temperature in the $BaCr_2As_2$ parent compound similarly to $BaMn_2As_2$ [23], which also exhibits a G-type AFM ordering of Mn moments at $T_N = 625$ K. Moreover, the closely related compounds *Ln*OCrAs possess similar CrAs layers, in which Cr ions bear a large itinerant moment of 1.57 μ_B and undergo a G-type AFM ordering with Néel temperature in between 300–550 K [28]. Similar magnetic ordering of Cr in $EuCr_2As_2$ is also possible at higher temperature.

C. Specific heat

Figure 4 shows the plots of temperature dependence of heat capacity $C_P(T)$ of the $EuCr_2As_2$ single crystal and that of the reference compound $BaCr_2As_2$ taken from Ref. [19]. The $C_P(T)$ of $EuCr_2As_2$ exhibits a sharp λ-type anomaly due to the magnetic transition at $T_m = 21$ K, indicating that the magnetic transition is of second order. The anomaly in $C_P(T)$ remains undisturbed under applied field of 500 Oe but with increasing field up to 5 kOe the anomaly is reduced significantly in height and considerably broadened suggesting a field-induced change of the nature of the magnetic transition, presumably a field-stabilized ferromagnetic order. The magnetic anomaly in the $C_P(T)$ makes it difficult to fit the data at lower temperature to extract the electronic specific-heat coefficient (γ). The

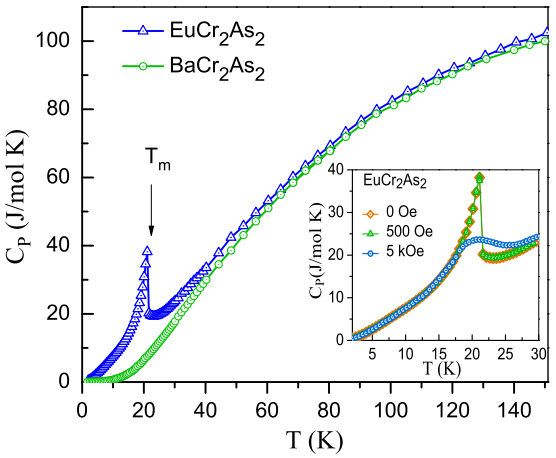

FIG. 4. (Color online) Temperature dependence of the specific heat C_P of $EuCr_2As_2$ single crystal and that of the reference compound $BaCr_2As_2$ taken from Ref. [19]. The lower inset shows the C_P of $EuCr_2As_2$ at zero field and under external fields of 500 Oe and 5 kOe.

measured value of $C_P(T)/T$ at 2 K is ≈225 mJ/mol K^2, but the estimation of γ from this value is not reliable as there are magnon contributions from the nearby magnetic ordering of Eu moments. A large $C_P(T)/T$ (≈250 mJ/mol K^2) at 2 K was also observed in ferromagnetically ordered $EuFe_2P_2$ [13].

The magnetic part of the heat capacity $C_{\rm mag}(T)$ was deduced by the usual method of subtracting the heat capacity of $BaCr_2As_2$ from that of $EuCr_2As_2$ after adjusting the renormalization due to different atomic masses of Ba and Eu, although the mass difference is small here. Based on the mean-field theory [36], the heat-capacity jump at the magnetic transition is calculated for the two possible magnetic structures: (i) the equal moment (EM) structure where the magnetic moments are the same at all sites and (ii) the amplitude modulated (AM) structure where the magnetic-moment amplitude varies periodically from one site to another. For EM structure, the jump in the heat capacity at the ordering temperature is given by [36]

$$\Delta C_{\rm EM} = 5\frac{J(J+1)}{(2J^2+2J+1)}R, \quad (1)$$

and for AM structure,

$$\Delta C_{\rm AM} = \frac{10}{3}\frac{J(J+1)}{(2J^2+2J+1)}R, \quad (2)$$

where J is the total angular momentum and R is the gas constant. By using $J = S = 7/2$ for divalent Eu, $\Delta C_{\rm EM}$ and $\Delta C_{\rm AM}$ amount to 20.15 J/mol K and 13.4 J/mol K, respectively. Our estimated ΔC (≈20.25 J/mol K) at T_m suggests that $EuCr_2As_2$ possesses an EM structure. In addition, a hump appears in the specific heat at $T \sim T_m/3$, which arises naturally within the mean-field theory for a $(2J+1)$-fold degenerate multiplet. The hump is seen in experimental $C_{\rm mag}(T)$ for $EuCr_2As_2$, which is more pronounced in the $C_{\rm mag}/T$ versus T plot (Fig. 5). The hump in the ordered state is particularly noticeable in compounds containing Eu^{2+} or Gd^{3+} with $S = 7/2$, and is not visible for lower S, e.g., $S = 1/2$ [36–38]. The magnetic contribution to the entropy

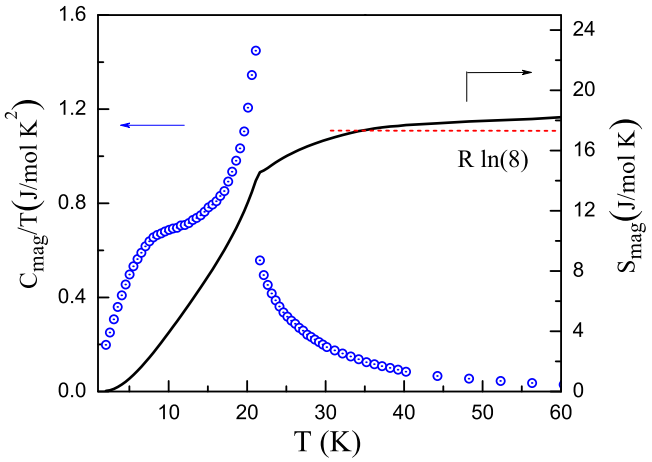

FIG. 5. (Color online) C_{mag}/T vs T of $EuCr_2As_2$ and the calculated magnetic entropy S_{mag} vs T shown by the solid line.

S_{mag} was obtained by integrating the C_{mag}/T versus T. The C_{mag}/T data were extrapolated from $T = 2$ K to $T = 0$ in order to approximate the missing C_{mag}/T data between 0 and 2 K. As can be seen from Fig. 5, the S_{mag} saturates to the expected theoretical value $R\ln(2S+1) = 17.3$ J/mol K, where $S = 7/2$ for Eu^{2+}. The magnetic entropy $S_{mag} = 14.6$ J/mol K at T_m is 84% of the theoretical value.

D. Transport properties

The temperature dependence of in-plane electrical resistivity $\rho_{ab}(T)$ of $EuCr_2As_2$ as shown in Fig. 6 exhibits a metallic behavior with residual resistivity $\rho_{ab} = 2.0\ \mu\Omega$ cm at 2 K and residual resistivity ratio RRR $= \rho_{300\,K}/\rho_{2\,K} \approx 90$. The high residual resistivity ratio together with a low residual resistivity confirms the high quality of our crystals. Since the compound is metallic, most likely the magnetic coupling between the Eu spins is mainly mediated by the conduction electrons through indirect Ruderman-Kittel-Kasuya-Yosida (RKKY) interaction. The resistivity data show a kink at the magnetic transition temperature (T_m) followed by a rapid decrease in resistivity below T_m due to reduction of spin disorder scattering. Further, we observe significant reduction of the electrical resistivity adjacent to the magnetic ordering temperature on application of magnetic field, leading to a negative magnetoresistance (MR). The MR reaches its maximum value (−24%) near T_m. The MR (Fig. 6) is defined as $[\rho(H) - \rho(0)]/\rho(0)$, where $\rho(0)$ and $\rho(H)$ are the resistivity measured at zero field and under applied field $H = 50$ kOe, respectively.

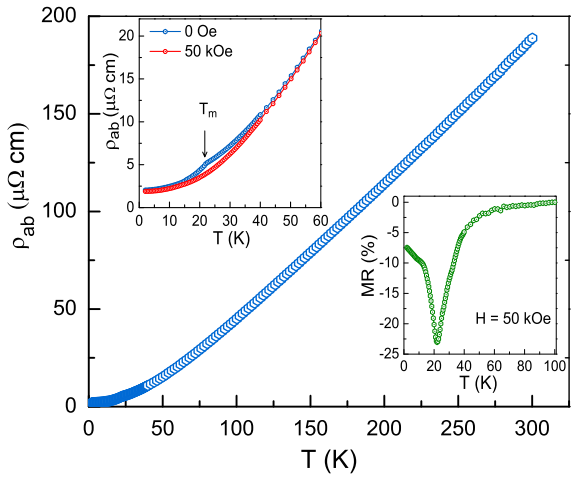

FIG. 6. (Color online) Temperature dependence of in-plane resistivity ρ_{ab} for $EuCr_2As_2$ under zero applied magnetic field. The upper inset shows an enlarged view of ρ_{ab} under applied magnetic fields of 0 and 50 kOe parallel to the c axis. The lower inset shows the temperature dependence of magnetoresistance for $EuCr_2As_2$.

E. Density functional calculations

In order to study the electronic and magnetic properties of the compound we start with the calculation of the density of states (DOS) for $EuCr_2As_2$ in the quenched paramagnetic state, that means no spin polarization is allowed on the Cr ions, but spin polarization is enabled for the Eu ions. Such a study can provide an intimation of magnetic state for the transition-metal ions by analyzing the partial density of states (PDOS) at the Fermi level and we can infer whether the magnetic state is favored or not. A similar approach was adopted in prior calculations for $EuFe_2As_2$ [12,31], the DOS of which is shown here for comparison purposes. We use the experimental lattice parameters $a = 3.893(2)$ Å and $c = 12.872(2)$ Å of $EuCr_2As_2$ for the calculations. The internal coordinate of As ($z_{As} = 0.361$) is determined by force minimization, which is very close to the experimental z_{As} for $EuCr_2As_2$. For the reference compound $EuFe_2As_2$, the experimental lattice parameters were taken from Ref. [9].

The general shape of our density of states for $EuCr_2As_2$ (Fig. 7) is similar to that for $EuFe_2As_2$, but with a shift of $3d$ orbitals in the binding energy, which is expected as Cr has two $3d$ electrons less as compared to Fe. The calculated DOS for $EuFe_2As_2$ is very similar to that reported by Li *et al.* [31].

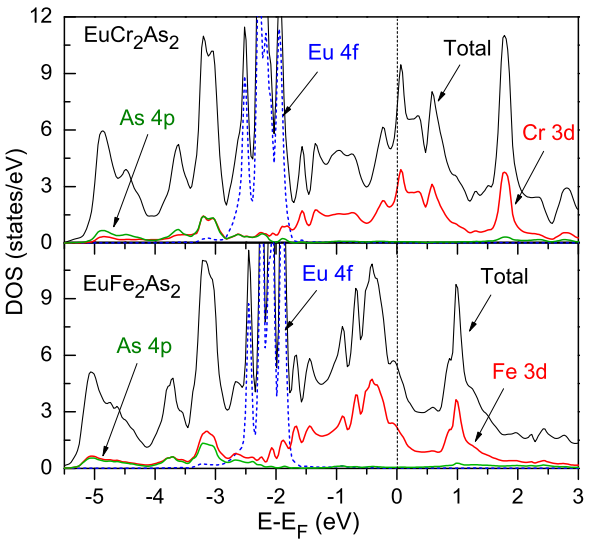

FIG. 7. (Color online) Total and partial densities of states (DOS) for $EuCr_2As_2$ and $EuFe_2As_2$ in the NM state in Cr/Fe sublattice and FM interaction between the intralayer Eu spins in the Eu sublattice.

The Eu $4f$ states for both the compounds are quite localized in between -1.5 to -3 eV, suggesting that the Eu ions are in a stable $2+$ valence state. The calculated spin moment for Eu^{2+} is about 6.9 μ_B which is consistent with the experimental value. The rest of the DOS can be divided into two parts: (i) The DOS below -2 eV consists of hybridized Cr $3d$ and As $4p$ orbitals. The p-d hybridization between As $4p$ and Cr $3d$ is sizable. (ii) The DOS near the Fermi level ranging from -2 eV to $+2$ eV is basically composed of the Cr $3d$ orbitals. The Fermi level lies on a steep edge of a peak in the partial density of states of Cr-$3d$ orbitals, resulting in a relatively large DOS at the Fermi energy. The corresponding value of PDOS at the Fermi level for Cr-$3d$ is $N(E_F) = 3.03$ states/eV per Cr atom, which is greater than that of Fe-$3d$ states (2.15 states/eV per Fe atom) in $EuFe_2As_2$ [31]. According to the Stoner criterion, magnetism may occur if $N(E_F)\, I > 1$, where I is the Stoner exchange-correlation integral [39]. We use the Stoner exchange-correlation integral $I = 0.38$ eV for Cr-$3d$ from the original work of Janak [40], which amounts to $N(E_F)\, I = 1.15$. Therefore, the nonmagnetic (NM) state of Cr is unstable against the magnetic order in $EuCr_2As_2$.

To examine the most stable magnetic structure of Cr in $EuCr_2As_2$, we have calculated the total energy for different possible magnetic states, namely, (i) a non-spin-polarized calculation (no magnetism on Cr), (ii) FM spin configuration, (iii) stripe-type AFM (similar to that in $EuFe_2As_2$), and (iv) G-type AFM (see Fig. 8). The corresponding total energies of different magnetic states together with the calculated moment values are listed in Table III. It is shown that a G-type AFM order in the Cr sublattice is the lowest energy state for $EuCr_2As_2$. The large energy differences between different Cr magnetic configurations suggest that the magnetic ordering temperature of Cr moments should be high. $BaCr_2As_2$ also possess a G-type AFM ground state of Cr itinerant moments as has been reported by Singh *et al.* [19]. Neutron diffraction studies on $BaFe_{2-x}Cr_xAs_2$ show a G-type AFM ground state for $x > 0.3$ [21]. Recent experimental investigation on the

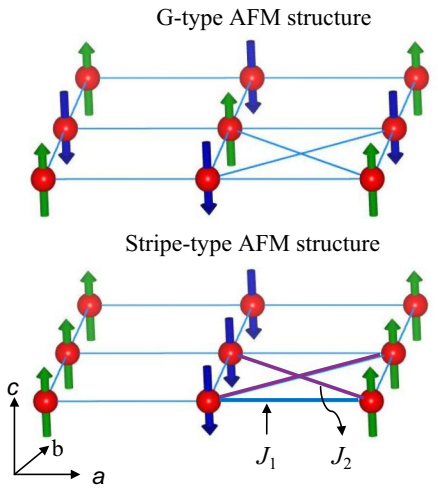

FIG. 8. (Color online) The top panel shows the G-type (Néel or checkerboard) AFM structure where nearest-neighbor spins are aligned antiparallel. The bottom panel represents stripe-type AFM ordering along with the definitions of the in-plane exchange constants J_1 and J_2.

TABLE III. Results of energetic and magnetic properties of $EuCr_2As_2$ for different magnetic states in the Cr sublattice and interlayer AFM coupling in the Eu sublattice. ΔE (eV) is the total energy difference per formula unit basis (two Cr atoms) with respect to the the non-spin-polarized or nonmagnetic state, and $m_{Cr}(\mu_B)/m_{Eu}(\mu_B)$ is the calculated magnetic moment on Cr/Eu. (NM = nonmagnetic or non-spin-polarized, FM = ferromagnetic, S-AFM = stripe-type AFM order, G-AFM = G-type AFM or checkerboard nearest-neighbor AFM order).

Cr ordering	ΔE (eV)	$m_{Cr}(\mu_B)/m_{Eu}(\mu_B)$
NM	0	0/6.9
FM	−0.136	1.28/6.9
S-AFM	−0.064	1.69/6.9
G-AFM	−0.417	2.10/6.9

closely related compound LaOCrAs reveals a G-type AFM order of Cr itinerant moments of 1.57 μ_B [28]. Therefore, our calculation of minimum ground state energy for a G-type AFM order of Cr moments in $EuCr_2As_2$ agrees with the magnetic structure of other related compounds. According to the Heisenberg model with nearest-neighbor (J_1) and next-nearest-neighbor (J_2) spin interactions, the differences in the ordered energies for several collinear commensurate magnetic structures are given by [41]

$$E_{FM} - E_{G-AFM} = 2NS^2(2J_1) \tag{3}$$

and

$$E_{G-AFM} - E_{S-AFM} = 2NS^2(2J_2 - J_1), \tag{4}$$

where N is the number of spins S. The in-plane G-type AFM is favored when $J_1 > 0$ and $J_1 > 2J_2$. Our calculations yield an antiferromagnetic J_1 (>0) and a large negative J_2 with $J_2/J_1 = -0.77$. The large negative value of J_2 implies that this model is probably not reliable for the system. This might be expected in an itinerant magnetic system with long-range magnetic order, as has been pointed out by Singh *et al.* for the $BaCr_2As_2$ system [19].

Experimentally we do not observe any signature of Cr moment ordering up to 300 K. This is not surprising considering the large total energy differences between different magnetic Cr moment configurations, which suggest an ordering temperature well above the maximum temperature of our measurements. Magnetic measurements at higher temperature are needed to corroborate the expected AFM ordering of Cr moments. The calculated magnetic structure of Cr moments can be verified experimentally using neutron or x-ray scattering measurements.

Finally, we discuss the magnetic order in the Eu sublattice. The calculated total energy for the system is found to be minimum when the interlayer Eu spins are antiferromagnetically coupled. Nevertheless, the difference in total energy is very small (∼0.0006 eV) whether the interlayer Eu spins are antiferromagnetically coupled or ferromagnetically coupled, implying a rather weak interlayer coupling in the Eu sublattice. So, it is expected that any small external effect (doping, external pressure, or external magnetic field) can easily flip the Eu spin from AFM to FM. The P-doped $EuFe_2As_2$ system witnesses a similar weak interlayer coupling (0–6 meV), wherein

the antiferromagnetic Eu moment arrangement changes from AFM to FM with slight change in doping concentration [33]. Furthermore, the homologous system $EuFe_2As_2$ with antiferromagnetic ground state experiences a field-induced spin reorientation to the FM state for an applied field of just 1 T in the ab plane and at 2 T along the c axis [34,35], which suggests a weak AFM coupling between the interlayer Eu spins. Taking into consideration the relatively large interlayer distance between the Eu layers along the c axis (6.44 Å for $EuCr_2As_2$, and 6.057 Å for $EuFe_2As_2$), the interlayer coupling of Eu spins in $EuCr_2As_2$ is expected to be even less.

IV. CONCLUSIONS

In summary, we have successfully synthesized single and poly crystals of $EuCr_2As_2$ and characterized them using x-ray diffraction, electrical resistivity $\rho(T)$, magnetization, and specific heat $C_p(T)$ measurements. The powder XRD data confirm that this compound crystallizes in the body-centered tetragonal structure (space group $I4/mmm$). The $C_p(T)$ and $\rho(T)$ data show anomalies at a temperature $T_m = 21$ K. While the susceptibility behavior apparently indicates a ferromagnetic order below 21 K, the magnetization data in the ordered state do not show any hysteresis or spontaneous magnetization. Furthermore, the value of θ_P obtained from the Curie-Weiss fit in the paramagnetic state is positive and very close to the magnetic transition temperature. These observations indicate that the dominant nearest-neighbor (i.e., intralayer) Eu-Eu interaction is FM but there could be a weak or frustrated AFM coupling between the layers. Also, we do not rule out the possibility of a FM state of Eu^{2+} moments in $EuCr_2As_2$. The measured saturated magnetization for both $H \parallel ab$ and $H \parallel c$ are larger than the theoretical value of $gS = 7.0\ \mu_B$ per Eu atom, suggesting that the Cr moments possibly contribute to the observed saturated magnetization values. The $\rho(T)$ data confirm the metallic state of $EuCr_2As_2$ with a negative magnetoresistance (-24%) around the magnetic transition. The magnetic entropy $S_{mag}(T)$ at T_m is 84% of the theoretical value $R\ln(2S+1)$ for $S = 7/2$ of the Eu^{2+} ion and the remaining 16% is recovered by ≈34 K. The electronic structure calculations indicate that the Cr ions carry itinerant moment and the most stable magnetic structure in the Cr sublattice is a G-type AFM order. Moreover, the large total energy differences between different magnetic Cr moment configurations suggest an ordering temperature well above the maximum temperature of our measurements. Higher temperature magnetic measurements are needed to observe the expected Cr moment ordering. Density functional calculations suggest a very weak interlayer coupling between the Eu moments. It would be useful and interesting to determine the magnetic structures of $EuCr_2As_2$ by magnetic neutron or x-ray scattering measurements.

ACKNOWLEDGMENT

This work has been partially supported by the Council of Scientific and Industrial Research, New Delhi [Grant No. 80(0080)/12/ EMR-II].

[1] M. Rotter, M. Tegel, and D. Johrendt, Phys. Rev. Lett. **101**, 107006 (2008).
[2] Kalyan Sasmal, Bing Lv, Bernd Lorenz, Arnold M. Guloy, Feng Chen, Yu-Yi Xue, and Ching-Wu Chu, Phys. Rev. Lett. **101**, 107007 (2008).
[3] Athena S. Sefat, Rongying Jin, Michael A. McGuire, Brian C. Sales, David J. Singh, and David Mandrus, Phys. Rev. Lett. **101**, 117004 (2008).
[4] H. S. Jeevan, Z. Hossain, Deepa Kasinathan, H. Rosner, C. Geibel, and P. Gegenwart, Phys. Rev. B **78**, 092406 (2008).
[5] C. F. Miclea, M. Nicklas, H. S. Jeevan, D. Kasinathan, Z. Hossain, H. Rosner, P. Gegenwart, C. Geibel, and F. Steglich, Phys. Rev. B **79**, 212509 (2009).
[6] R. Nagarajan, G. K. Shenoy, L. C. Gupta, and E. V. Sampathkumaran, Phys. Rev. B **32**, 2846 (1985).
[7] Y. Hiranaka, A. Nakamura, M. Hedo, T. Takeuchi, A. Mori, Y. Hirose, K. Mitamura, K. Sugiyama, M. Hagiwara, T. Nakama, and Y. Ōnuki, J. Phys. Soc. Jpn. **82**, 083708 (2013).
[8] B. C. Sales and R. Viswanathan, J. Low Temp. Phys. **23**, 449 (1976).
[9] H. S. Jeevan, Z. Hossain, Deepa Kasinathan, H. Rosner, C. Geibel, and P. Gegenwart, Phys. Rev. B **78**, 052502 (2008).
[10] S. Zapf, D. Wu, L. Bogani, H. S. Jeevan, P. Gegenwart, and M. Dressel, Phys. Rev. B **84**, 140503(R) (2011).
[11] Anupam, V. K. Anand, P. L. Paulose, S. Ramakrishnan, C. Geibel, and Z. Hossain, Phys. Rev. B **85**, 144513 (2012).
[12] U. B. Paramanik, Debarchan Das, R. Prasad, and Z. Hossain, J. Phys.: Condens. Matter **25**, 265701 (2013).
[13] C. Feng, Z. Ren, S. Xu, S. Jiang, Z. Xu, I. Nowik, I. Felner, G. Cao, K. Matsubayashi, and Y. Uwatoko, Phys. Rev. B **82**, 094426 (2010).
[14] D. H. Ryan, J. M. Cadogan, S. Xu, Z. Xu, and G. Cao, Phys. Rev. B **83**, 132403 (2011).
[15] Yogesh Singh, Y. Lee, B. N. Harmon, and D. C. Johnston, Phys. Rev. B **79**, 220401(R) (2009).
[16] Kausik Sengupta, P. L. Paulose, E. V. Sampathkumaran, Th. Doert, and J. P. F. Jemetio, Phys. Rev. B **72**, 184424 (2005).
[17] E. D. Bauer, F. Ronning, B. L. Scott, and J. D. Thompson, Phys. Rev. B **78**, 172504 (2008).
[18] J. Ballinger, L. E. Wenger, Y. K. Vohra, and A. S. Sefat, J. Appl. Phys. **111**, 07E106 (2012).
[19] D. J. Singh, A. S. Sefat, M. A. McGuire, B. C. Sales, D. Mandrus, L. H. Van Bebber, and V. Keppens, Phys. Rev. B **79**, 094429 (2009).
[20] A. S. Sefat, D. J. Singh, L. H. Van Bebber, Y. Mozharivskyj, M. A. McGuire, R. Jin, B. C. Sales, V. Keppens, and D. Mandrus, Phys. Rev. B **79**, 224524 (2009).
[21] K. Marty, A. D. Christianson, C. H. Wang, M. Matsuda, H. Cao, L. H. Van Bebber, J. L. Zarestky, D. J. Singh, A. S. Sefat, and M. D. Lumsden, Phys. Rev. B **83**, 060509(R) (2011).
[22] Yogesh Singh, A. Ellern, and D. C. Johnston, Phys. Rev. B **79**, 094519 (2009).

[23] Yogesh Singh, M. A. Green, Q. Huang, A. Kreyssig, R. J. McQueeney, D. C. Johnston, and A. I. Goldman, Phys. Rev. B **80**, 100403(R) (2009).
[24] Abhishek Pandey, R. S. Dhaka, J. Lamsal, Y. Lee, V. K. Anand, A. Kreyssig, T. W. Heitmann, R. J. McQueeney, A. I. Goldman, B. N. Harmon, A. Kaminski, and D. C. Johnston, Phys. Rev. Lett. **108**, 087005 (2012).
[25] A. T. Satya, Awadhesh Mani, A. Arulraj, N. V. Chandra Shekar, K. Vinod, C. S. Sundar, and A. Bharathi, Phys. Rev. B **84**, 180515(R) (2011).
[26] Abhishek Pandey, B. G. Ueland, S. Yeninas, A. Kreyssig, A. Sapkota, Yang Zhao, J. S. Helton, J. W. Lynn, R. J. McQueeney, Y. Furukawa, A. I. Goldman, and D. C. Johnston, Phys. Rev. Lett. **111**, 047001 (2013).
[27] R. Ruehl and W. Jeitschko, Mater. Res. Bull. **14**, 513 (1979).
[28] S.-W. Park, H. Mizoguchi, K. Kodama, S.-i. Shamoto, T. Otomo, S. Matsuishi, T. Kamiya, and H. Hosono, Inorg. Chem. **52**, 13363 (2013).
[29] P. Blaha, K. Schwarz, G. K. H. Madsen, D. Kvasnicka, and J. Luitz, *WIEN2k, An Augmented Plane Wave Plus Local Orbitals Program for Calculating Crystal Properties* (Vienna University of Technology, Vienna, 2001).
[30] J. P. Perdew, K. Burke, and M. Ernzerhof, Phys. Rev. Lett. **77**, 3865 (1996).
[31] Wei Li, Jian-Xin Zhu, Yan Chen, and C. S. Ting, Phys. Rev. B **86**, 155119 (2012).
[32] D. Givord, H. S. Li, and R. Perrier de la Bâthie, Solid State Commun. **51**, 857 (1984).
[33] H. S. Jeevan, Deepa Kasinathan, Helge Rosner, and Philipp Gegenwart, Phys. Rev. B **83**, 054511 (2011).
[34] S. Jiang, Y. Luo, Z. Ren, Z. Zhu, C. Wang, X. Xu, Q. Tao, G. Cao, and Z. Xu, New J. Phys. **11**, 025007 (2009).
[35] Y. Xiao, Y. Su, W. Schmidt, K. Schmalzl, C. M. N. Kumar, S. Price, T. Chatterji, R. Mittal, L. J. Chang, S. Nandi, N. Kumar, S. K. Dhar, A. Thamizhavel, and Th. Brueckel, Phys. Rev. B **81**, 220406(R) (2010).
[36] J. A. Blanco, D. Gignoux, and D. Schmitt, Phys. Rev. B **43**, 13145 (1991).
[37] D. C. Johnston, R. J. McQueeney, B. Lake, A. Honecker, M. E. Zhitomirsky, R. Nath, Y. Furukawa, V. P. Antropov, and Y. Singh, Phys. Rev. B **84**, 094445 (2011).
[38] R. J. Goetsch, V. K. Anand, and D. C. Johnston, Phys. Rev. B **87**, 064406 (2013).
[39] D. J. Singh, Phys. Rev. B **78**, 094511 (2008).
[40] J. F. Janak, Phys. Rev. B **16**, 255 (1977).
[41] David C. Johnston, Adv. Phys. **59**, 803 (2010).
[42] H. Raffius, E. Mörsen, B. D. Mosel, W. Müller-Warmuth, W. Jeitschko, L. Terbüchte, and T. Vomhof, J. Phys. Chem. Solid **54**, 135 (1993).